

Search for Supersymmetry Using Diphoton Events in $p\bar{p}$ Collisions at $\sqrt{s} = 1.96$ TeV

Eunsin Lee (for CDF Collaboration)

Department of Physics, Texas A&M University, College Station, TX 77843, USA

We present the results of a search for supersymmetry with gauge-mediated breaking and $\tilde{\chi}_1^0 \rightarrow \gamma\tilde{G}$ in the $\gamma\gamma$ +missing transverse energy final state. In 2.6 ± 0.2 fb $^{-1}$ of $p\bar{p}$ collisions at $\sqrt{s}=1.96$ TeV recorded by the CDF II detector we observe no candidate events, consistent with a standard model background expectation of 1.4 ± 0.4 events. We set limits on the cross section at the 95% C.L. and place the world's best limit of 149 GeV/ c^2 on the $\tilde{\chi}_1^0$ mass at $\tau_{\tilde{\chi}_1^0} \ll 1$ ns. We also exclude regions in the $\tilde{\chi}_1^0$ mass-lifetime plane for $\tau_{\tilde{\chi}_1^0} \lesssim 2$ ns.

1. Introduction

For theoretical reasons [1], and because of the ‘ $e\bar{e}\gamma\gamma$ +missing transverse energy (\cancel{E}_T)’ candidate event recorded by the CDF detector in RUN I [2], there is a compelling rationale to search in high energy collisions for the production of heavy new particles that decay producing the signature of $\gamma\gamma + \cancel{E}_T$.

An example of a theory that would produce such events is gauge mediated supersymmetry breaking (GMSB) [1] with $\tilde{\chi}_1^0 \rightarrow \gamma\tilde{G}$ where the $\tilde{\chi}_1^0$ is the lightest neutralino and the next-to-lightest supersymmetric particle (NLSP) and the \tilde{G} is a gravitino which is the lightest supersymmetric particle (LSP), giving rise to \cancel{E}_T by leaving the detector without depositing any energy. The \tilde{G} also provides a warm dark matter candidate that is both consistent with inflation and astronomical observations [3].

In these models, above the current limits from recent experiments [4], the $\tilde{\chi}_1^0$ is restricted to be well above 100 GeV and is favored to have a lifetime on the order of a nanosecond; the \tilde{G} is restricted to have a mass in the range $0.5 < m_{\tilde{G}} < 1.5$ keV/ c^2 [5]. At the Tevatron sparticle production is predicted to be primarily into gaugino pairs, and the $\tilde{\chi}_1^0$ mass ($m_{\tilde{\chi}_1^0}$) and lifetime ($\tau_{\tilde{\chi}_1^0}$) are the two most important parameters in determining the final states and their kinematics [1]. Depending on how many of the two $\tilde{\chi}_1^0$'s decay inside the detector, the event has the signature $\gamma\gamma + \cancel{E}_T$, $\gamma + \cancel{E}_T$ or \cancel{E}_T with one or more additional high E_T particles from the other gaugino pairs. Different search strategies are required for $\tilde{\chi}_1^0$ lifetimes above and below about a nanosecond [9]. Previous searches have been performed for low lifetime models in $\gamma\gamma + \cancel{E}_T$ [6, 7] and nanosecond lifetime models in the delayed $\gamma + jet + \cancel{E}_T$ [4, 8] final state.

In this analysis we focus on the $\gamma\gamma + \cancel{E}_T$ final state, as recommended in [9], for low lifetime, high-mass models of the $\tilde{\chi}_1^0$. The new features of our analysis since the last $\gamma\gamma + \cancel{E}_T$ search with 202 pb $^{-1}$ using the CDF detector [10] are to use the EMTiming system [11] and a new *Met Resolution Model* [12]. We also use 13 times the data (2.6 fb $^{-1}$). These additions significantly enhance our rejection of backgrounds from

instrumental and non-collision sources, which allows us to considerably extend the sensitivity of the search for large $\tilde{\chi}_1^0$ masses compared to previous Tevatron searches [7]. We also extend the search by considering $\tilde{\chi}_1^0$ lifetimes up to 2 ns which are favored for larger $m_{\tilde{\chi}_1^0}$.

Our analysis begins by defining a preselection sample by selecting events with two isolated, central ($|\eta| \lesssim 1.0$) photons with $E_T > 13$ GeV. All candidates are required to pass the standard CDF diphoton triggers, global event selection, standard photon ID, and non-collision background rejection requirements [6, 12].

The final signal region for this analysis is defined by the subsample of preselection events that also pass a set of optimized final kinematic requirements. The methods for determining the background in the signal region are based on a combination of data and Monte Carlo (MC) simulation and allow for a large variety of potential final sets of kinematic requirements. We perform an *a priori* analysis in the sense that we blind the signal region and select the final event requirements based on the signal and background expectations alone. We optimize our predicted sensitivity using a simulation of our GMSB model. We then calculate, for each GMSB parameter point, the lowest, expected 95% C.L. cross section limit in the no-signal scenario [14] as a function of the following event variables: $MetSig$, $\Delta\phi(\gamma_1, \gamma_2)$, and H_T , each of which will be described in Section 5.

2. Data Selection

The analysis is based on 2.59 ± 0.16 fb $^{-1}$ of data delivered to the CDF detector in Run II. The analysis selection begins with events that pass the CDF diphoton triggers which is effectively 100% efficient for the final diphoton selection requirements [12]. We require both highest- E_T photons to be in the fiducial part of the detector with $|\eta| \leq 1.1$, pass the standard photon ID and isolation requirements and have $E_T^\gamma > 13$ GeV. In addition to the standard photon ID requirements we have added additional requirements to suppress

photomultiplier tube (PMT) high-voltage breakdowns (“spikes”) [8] and electron rejection requirements [8] to remove events where an electron fakes a prompt photon (Phoenix tracking rejection). Each event is required to have at least one high quality vertex with $|z_{vx}| \leq 60$ cm. The E_T of all calorimeter objects (individual towers, photons, electrons, and jets) are calculated with respect to the highest $\sum P_T$ vertex. However, an incorrect vertex can be selected when two or more collisions occur in one beam-bunch crossing, making it possible that the highest reconstructed $\sum P_T$ vertex does not produce the photons. If assigning the photons to a different vertex lowers the \cancel{E}_T , we take that \cancel{E}_T and the photon E_T 's to be from that vertex for all calculations (Vertex Re-assignment).

Additional standard selection requirements are placed to reduce non-collision backgrounds, such as cosmic rays and beam-related (beam halo) effects [8]. We also apply \cancel{E}_T quality requirements (cleanup) to remove events if there is evidence that the second photon (γ_2) or a jet is partially lost in a crack between detector components [12]. Our pre-selection sample consists of 38,053 events left after all the quality, ID and cleanup requirements are applied [12].

3. Backgrounds

There are three major sources of background for $\gamma\gamma + \cancel{E}_T$ events: QCD events with fake \cancel{E}_T , electroweak events with real \cancel{E}_T , and non-collision events (PMT spikes, cosmic ray or beam-halo events where one or more of the photons and \cancel{E}_T are not related to the collision).

Standard Model QCD sources, $\gamma\gamma$, $\gamma - jet \rightarrow \gamma\gamma_{fake}$, and $jet - jet \rightarrow \gamma_{fake}\gamma_{fake}$, are the dominant producer of events in the diphoton final state and a major background for $\gamma\gamma$ with fake \cancel{E}_T . These backgrounds come in two different categories; fake \cancel{E}_T due to energy measurement fluctuations in the calorimeter and fake \cancel{E}_T due to pathologies such as picking the wrong vertex in events where the true collision did not create a vertex or tri-photon events with a lost photon.

To estimate the background due to energy measurement fluctuations we use the *Met Resolution Model*. The *Met Resolution Model* considers the clustered and unclustered energy in the event and calculates a probability, $P(\cancel{E}_T^{fluct} > \cancel{E}_T)$, for fluctuations in the energy measurement to produce \cancel{E}_T^{fluct} equivalent to or larger than the measured \cancel{E}_T . This probability is then used to define $MetSig = -\log_{10}(P_{\cancel{E}_T^{fluct} > \cancel{E}_T})$. Events with true and fake \cancel{E}_T of the same value should have, on average, different $MetSig$. For each data event we throw 10 pseudo-experiments to generate a \cancel{E}_T and calculate its significance, according to the jets and underlying event configuration. Then we count the num-

ber of events in the pseudo-experiments that pass our $MetSig$ and other kinematic requirements. This number, divided by the number of pseudo-experiments, gives us the *Met Model* prediction for a sample. The systematic uncertainty on the number of events above a $MetSig$ cut is evaluated by comparing the *Met Model* predictions with the default set of model parameters to predictions obtained with the parameters deviated by $\pm\sigma$. The total uncertainty is estimated by adding the statistical uncertainty on the number of pseudo-experiments passing the cuts and these systematic uncertainties in quadrature.

A source of QCD background that is unaccounted for by the *Met Model* is diphoton candidate events with event reconstruction pathologies such as a wrong choice of the primary interaction vertex or tri-photon events with a lost photon. To obtain the prediction for the number of events with significant reconstruction pathologies in the QCD background at the same time, we model the kinematics and event reconstruction using a MC simulation of events with in the detector using PYTHIA [15] and a GEANT-based detector simulation [16]. We simulate a sample of SM $\gamma\gamma$ events, with large statistics, and normalize to the number of events in the presample to take into account jet backgrounds which should have similar detector response. Then we subtract off the expectations for energy measurement fluctuations in the MC to avoid double counting. The remaining prediction is due to pathologies alone. The systematic uncertainties on this background prediction include the uncertainty on the scale factor and the uncertainty due to MC-data differences in the unclustered energy parameterization and the jet energy scale.

Electroweak processes involving W 's and Z 's are the most common source of real and significant \cancel{E}_T in $p\bar{p}$ collisions. We estimate the background rate from decays into both charged and neutral leptons using a combination of data and MC methods. There are four ways we can get a $\gamma\gamma + \cancel{E}_T$ signature in electroweak events that decay into one or more leptons: 1) from $W\gamma\gamma$ and $Z\gamma\gamma$ events where both photons are real; 2) from $W\gamma$ and $Z\gamma$ events with a fake photon; 3) from W and Z events where both photon candidates are fake photons; and 4) $t\bar{t}$ production and decay. To estimate the contribution from the electroweak backgrounds we use the Baur [17] and PYTHIA MC's along with a detector simulation, according to their production cross section and k-factors (the ratio of the next-to-leading order (NLO) cross section to the leading order cross section), but normalized to data. To minimize the dependence of our predictions on potential “MC-data” differences, we normalize, using the rate of the number of $e\gamma$ events observed in the data that also pass all signal kinematic cuts, to the number of events observed in MC. This $e\gamma$ sample is derived from diphoton trigger datasets and the events are required to pass the preselection requirements where electrons

are required to pass photon-like ID requirements [12]. The uncertainty on the electroweak backgrounds are dominated by the $e\gamma$ normalization factor uncertainty. This includes data and MC statistical uncertainties as well as differences in MC modeling. The total uncertainties also include the MC statistical uncertainties and uncertainties on the normalization factors added in quadrature.

Non-collision backgrounds coming from cosmic rays and beam-related effects can produce $\gamma\gamma + \cancel{E}_T$ candidates [8]. These are estimated using the data. Using the inclusive $\gamma\gamma$ sample selection requirements, but requiring one of the photons to have $t_\gamma > 25$ ns we identify a cosmic-enhanced sample. Similarly, we utilize a beam-related background enhanced sample. We estimate the number of these events in the signal region using the ratio of events outside the timing requirements to events inside the signal region and the measured efficiencies of the non-collision rejection requirements [12]. The uncertainties on both non-collision background estimates are dominated by the statistical uncertainty on the number of identified events.

After estimating the MetSig distributions for all the backgrounds, where the QCD is normalized to the data in the low MetSig region where the EWK backgrounds are expected to be negligible, the expected MetSig distribution for the presample is shown in Figure 1. With these tools in hand we are set to estimate the backgrounds for a large variety of kinematic requirements and move to an estimation of the acceptance for GMSB models in the signal region for use in optimization.

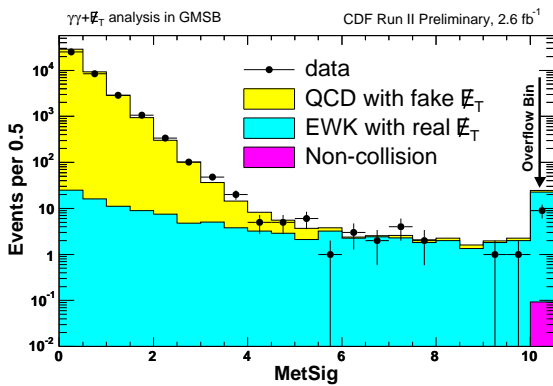


Figure 1: The background predictions of MetSig for the presample. The highest MetSig bin includes all overflow events.

4. GMSB Signal Monte Carlo and Systematic Uncertainties

To estimate the acceptance for GMSB we use the PYTHIA event generator as well as a full detector sim-

ulation. For the purpose of this analysis we consider a GMSB model with parameters fixed on the minimal-GMSB Snowmass slope constraint (SPS 8) that is commonly used [4, 6] and take the messenger mass scale $M_m = 2\Lambda$, $\tan(\beta) = 15$, $\mu > 0$ and the number of messenger fields $N_m = 1$. The \tilde{G} mass factor and the supersymmetry breaking scale Λ are allowed to vary independently. All SUSY production processes are simulated to maximize our sensitivity to the model [18].

Since we estimate the sensitivity of the search to be equal to the expected 95% C.L. cross section limits with the no signal hypothesis, we need the uncertainties for the luminosity, background and acceptance. The systematic uncertainty on the luminosity is taken to be 6% with major contributions from the uncertainties on the CLC acceptance from the precision of the detector simulation [16] and the event generator [15]. The background uncertainty is evaluated for every set of cuts in the optimization procedure. The systematic uncertainty on the signal acceptance for an example GMSB point of $m(\tilde{\chi}_1^0) = 140$ GeV and $\tau(\tilde{\chi}_1^0) \ll 1$ ns is estimated to be 6.9% with major contributions from diphoton ID and isolation efficiency (5.4%) and ISR/FSR (3.9%). The uncertainty on the NLO production cross section is dominated by the uncertainty from parton distribution functions (7.6%) and the renormalization scale (2.6%) for a total of 8.0%. All uncertainties are included in the final cross section limit calculation, and we take the acceptance and production cross section uncertainties in quadrature for a total uncertainty of 10.6%.

5. Optimization and Results

Now that the background is estimated and the signal acceptance is available for a variety of selection requirements, an optimization procedure can be readily employed to find the optimal selection requirements before unblinding the signal region. We optimize for the following kinematic requirements: MetSig, H_T , and $\Delta\phi(\gamma_1, \gamma_2)$.

As described in earlier section, the MetSig cut gets rid of most of the QCD background with fake \cancel{E}_T . The H_T cut separates between the high E_T , light final state particles produced by GMSB events via cascade decays and SM backgrounds, dominated by QCD and electroweak backgrounds, which do not have lots of high E_T objects. The $\Delta\phi(\gamma_1, \gamma_2)$ cut gets rid of events where two photons are back to back since electroweak backgrounds with large H_T are typically a high E_T photon recoiling against $W \rightarrow e\nu$, which means the gauge boson decay is highly boosted. Also the high E_T diphoton with large H_T from QCD background are mostly back-to-back with fake \cancel{E}_T or wrong vertex.

By estimating our sensitivity using the 95% C.L. expected cross section limits on GMSB models in the

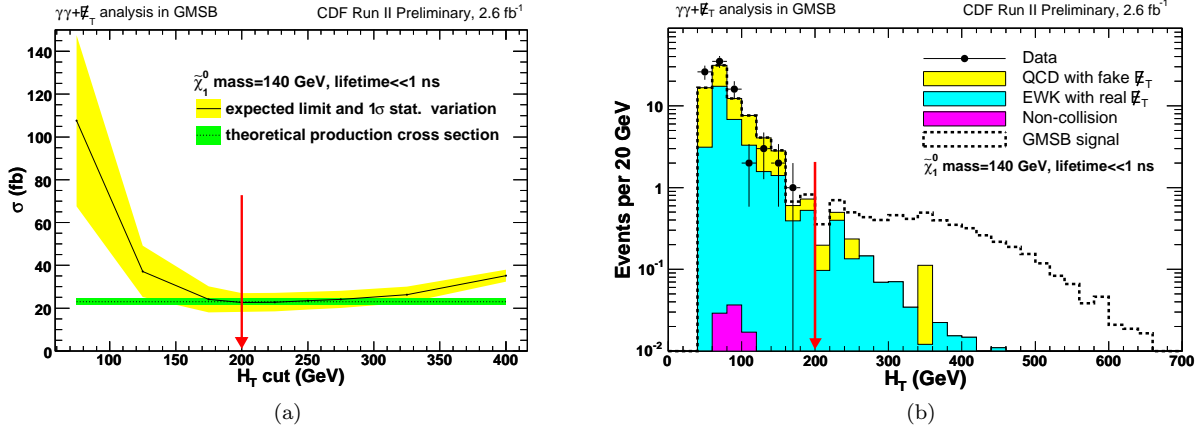


Figure 2: The expected 95% C.L. cross section limit as a function of the H_T (a) requirement for a GMSB example point ($m(\tilde{\chi}_1^0) = 140$ GeV and $\tau(\tilde{\chi}_1^0) \ll 1$ ns). All other cuts held at their optimized values. The optimal cut is where the expected cross section is minimized. Indicated in green is the 8.0% uncertainty-band for the production cross section and in yellow is the RMS. The N-1 predicted kinematic distribution along with data after the optimized requirements are shown in Figure (b). There is no evidence for new physics and the data is well modeled by backgrounds alone.

no-signal assumption, we find the optimal set of cuts before unblinding the signal region. We use the standard CDF cross section limit calculator [19] to calculate the limits, taking into account the predicted number of background events, the acceptance, the luminosity and their systematic uncertainties.

For each GMSB point the minimum expected cross section limit defines our set of optimal requirements for the mass and lifetime combination. The exclusion region is defined by the region where the production cross section is above the 95% C.L. cross section limit. The mass/lifetime limit is where the two cross. Figure 2-(a) shows the expected cross section limit as a function of a kinematic selection requirement after keeping all other requirements fixed at the already optimized values, showing it is at the minimum for a mass-lifetime combination of $m(\tilde{\chi}_1^0) = 140$ GeV and $\tau(\tilde{\chi}_1^0) \ll 1$ ns, which is near the exclusion region limit.

We decided to use a single set of optimal requirements before we open the box based on the observation that they will yield the largest expected exclusion region. We chose: $\text{MetSig} > 3$, $H_T > 200$ GeV, $\Delta\phi(\gamma_1, \gamma_2) < \pi - 0.35$ rad. With these requirements we predict a total of 1.38 ± 0.44 background events. The dominant electroweak contributions are $Z\gamma \rightarrow \nu\nu\gamma$ and $Z\gamma \rightarrow \mu\mu\gamma$ which produce a total of 0.26 ± 0.08 and 0.19 ± 0.10 events respectively. The QCD background is dominated by energy measurement fluctuations in the \cancel{E}_T , estimated using the *Met Model*, to have a rate of 0.46 ± 0.24 events. The non-collision backgrounds are dominated by cosmic ray which have a rate of $0.001^{+0.008}_{-0.001}$ events.

After all optimal cuts we open the box and observe no events, consistent with the expectation of 1.2 ± 0.4 events. We show the kinematic distributions for the background and signal expectations along with the

data in Figure 2-(b). There is no distribution that hints at an excess and the data appears to be well modeled by the background prediction alone.

We show the predicted and observed cross section limits along with the NLO production cross section, which is calculated by multiplying the PYTHIA LO cross section calculation by k-factor [20] in Figure 3. Since the number of observed events is below expectations the observed limits are slightly better than the expected limits. The $\tilde{\chi}_1^0$ mass reach, based on the predicted (observed) number of events is 141 GeV/ c^2 (149 GeV/ c^2), at a lifetime below 2 ns [9]. We show the 95% C.L. NLO exclusion region as a function of mass and lifetime of $\tilde{\chi}_1^0$ using the fixed choice of cuts from the optimization for both for the predicted and observed number of background events in Figure 4-(a). These limits extend the reach beyond the CDF delayed photon results [8] and well beyond those of $D\bar{O}$ searches at $\tau_{\tilde{\chi}_1^0} \ll 0$ [7] and the limit from ALEPH/LEP [4], and are currently the world's best.

6. Conclusions and Prospects for the future

We have set limits on GMSB models using the $\gamma\gamma + \cancel{E}_T$ final state. Candidate events were selected based on 13 times more data, the new \cancel{E}_T resolution model technique, the EMTiming system and a full optimization procedure. We found 0 events using 2.6 fb^{-1} of data in run II which is consistent with the background estimate of 1.2 ± 0.4 events from the Standard Model expectations. We showed exclusion regions and set limits on GMSB models with a $\tilde{\chi}_1^0$ mass reach of 149 GeV/ c^2 at a $\tilde{\chi}_1^0$ lifetime much less

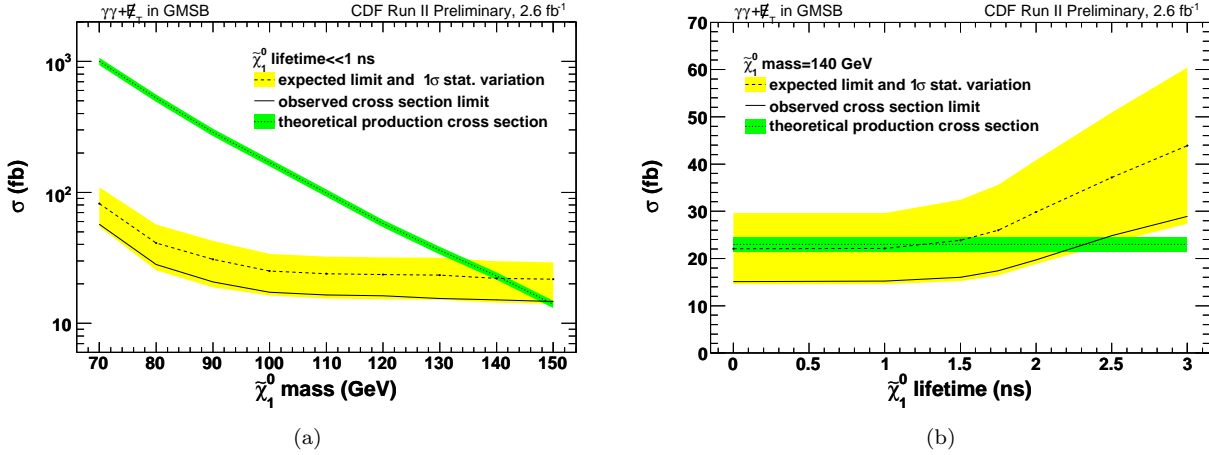


Figure 3: The predicted and observed cross section limits as a function of the $\tilde{\chi}_1^0$ mass at a lifetime much less than 1 ns (a) and as a function of the $\tilde{\chi}_1^0$ lifetime at a mass of 140 GeV/ c^2 (b). Indicated in green is the 8.0% uncertainty-band for the production cross section, in yellow the RMS variation in the expected on the cross section limit.

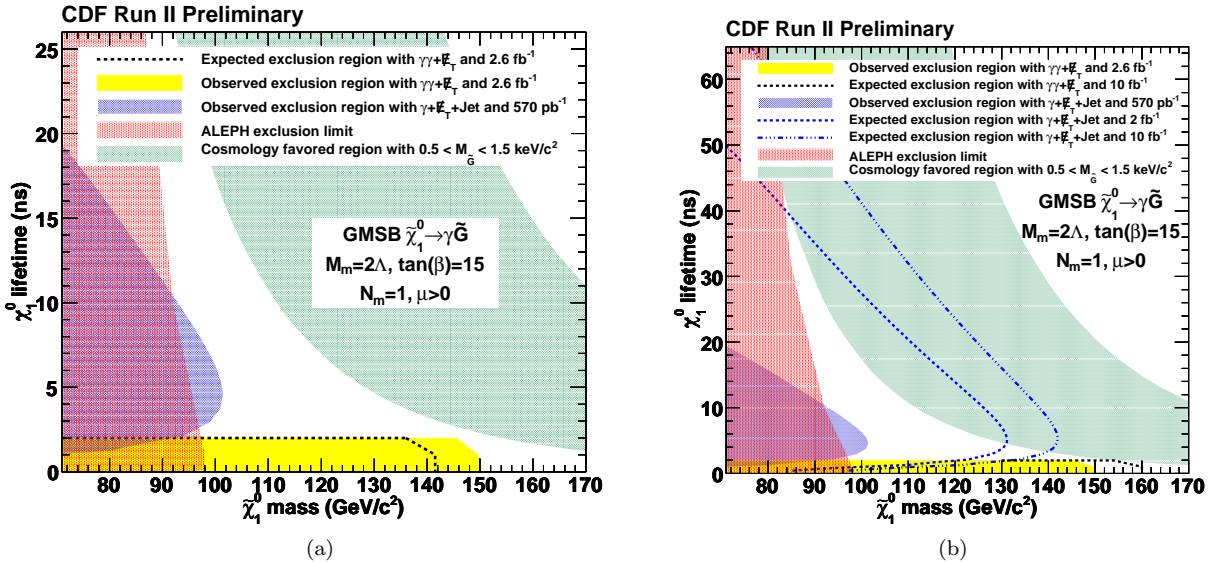


Figure 4: The predicted and observed exclusion region along with the limit from ALEPH/LEP [4] and the $\gamma + \cancel{E}_T + jet$ delayed photon analysis [8]. We have a mass reach of 141 GeV/ c^2 (predicted) and 149 GeV/ c^2 (observed) at the lifetime up to 1 ns. The green shaded band shows the parameter space where $0.5 < m_{\tilde{G}} < 1.5 \text{ keV}/c^2$, favored in cosmologically consistent models [5] (a). The projected sensitivity to GMSB models with more data. The black dashed line shows the prediction of the exclusion region limit after a scaling of the background prediction and the uncertainties for a luminosity of 10 fb^{-1} . The blue dashed lines show the prediction of the exclusion region limits from the delayed photon analysis for a luminosity of 2 fb^{-1} and 10 fb^{-1} respectively taken from Ref. [8]. (b)

than 1 ns. Our results extend the world sensitivity to these models.

To investigate the prospects of a search at higher luminosity we calculate the cross section limits assuming all backgrounds scale linearly with luminosity while their uncertainty fractions remain constant. By the end of Run II, with an integrated luminosity of 10 fb^{-1} , we estimate a mass reach of $\simeq 160 \text{ GeV}/c^2$ at a lifetime much less than 1 ns, as shown in Figure 4-

(b). For higher lifetimes (above ~ 2 ns) the next generation delayed photon analysis will extend the sensitivity taken from Ref. [8] and then will combine these results for completeness.

Acknowledgments

Eunsin Lee would like thank D. Toback, R. Culbertson, A. Pronko, M. D'onofrio, T. Wright for their help on this analysis and the talk.

References

- [1] S. Dimopoulos, S. Thomas, and J. Wells, Nucl. Phys. B **488**, 39 (1997); S. Ambrosanio, G. Kribs, and S. Martin, Phys. Rev. D **56**, 1761 (1997); G. Giudice and R. Rattazzi, Phys. Rep. **322**, 419 (1999); S. Ambrosanio, G. Kane, G. Kribs, S. Martin, and S. Mrenna, Phys. Rev. D **55**, 1372 (1997).
- [2] CDF Collaboration, F. Abe *et al.*, Phys. Rev. Lett. **81**, 1791 (1998); Phys. Rev. D **59**, 092002 (1999).
- [3] P. Bode, J. Ostriker, and N. Turok, Astrophys. J. **556**, 93 (2001).
- [4] ALEPH Collaboration, A. Heister *et al.*, Eur. Phys. J. C **25**, 339 (2002); A. Garcia-Bellido, Ph.D. thesis, Royal Holloway University of London (2002) (unpublished), arXiv:hep-ex/0212024.
- [5] C.-H. Chen and J. F. Gunion, Phys. Rev. D **58**, 075005 (1998).
- [6] CDF Collaboration, D. Acosta *et al.*, Phys. Rev. D **71**, 031104 (2005).
- [7] DØ Collaboration, V.M. Abazov *et al.*, Phys. Lett. B **659**, 856 (2008).
- [8] CDF Collaboration, A. Abdulencia *et al.*, Phys. Rev. Lett. **99**, 121801 (2007); CDF Collaboration, T.Aaltonen *et al.*, Phys. Rev. D **78**, 032015 (2008).
- [9] P. Wagner and D. Toback, Phys. Rev. D **70**, 114032 (2004).
- [10] D. Acosta *et al.* (CDF Collaboration), Phys. Rev. D **71**, 032001 (2005).
- [11] M. Goncharov *et al.*, NIM A**565**, 543 (2006).
- [12] T. Aaltonen *et al.* (CDF Collaboration), *Search for Anomalous Production of Events with Two Photons and Additional Energetic Objects at CDF*, to be submitted to Phys. Rev. D.
- [13] For a discussion of the jet energy measurements, see T. Affolder *et al.* (CDF Collaboration), Phys. Rev. D. **64**, 032001 (2001). For a discussion of standard jet correction systematics, see A. Bhatti *et al.*, Nucl. Instrum. Methods, A **566**, 375 (2006). We use jets with cone size $\Delta R=0.4$.
- [14] E. Boos, A. Vologdin, D. Toback and J. Gaspard, Phys. Rev. D **66**, 013011 (2002).
- [15] T. Sjöstrand *et al.*, Comput. Phys. Commun. **135**, 238 (2001). We use version 6.216.
- [16] We use the standard GEANT based detector simulation [R. Brun *et al.*, CERN-DD/EE/84-1 (1987)] and add a parametrized EMTiming simulation.
- [17] U. Baur, T. Han and J. Ohnemus, Phys. Rev. D **48**, 5140 (1993); U. Baur, T. Han and J. Ohnemus, *ibid.* **57**, 2823 (1998); The $W\gamma$ and $Z\gamma$ processes are simulated using the leading-order event generator and have a k-factor fixed at 1.36. Initial and final state radiation (resulting in additional jets or photons), underlying event, and additional interactions are simulated using PYTHIA [15].
- [18] P. Simeon and D. Toback, J. Undergrad. Research in Phys. **20**, 1 (2007).
- [19] T. Junk, Nucl. Instrum. Methods A**434**, 435-443 (1999).
- [20] W. Beenakker, *et al.*, Phys. Rev. Lett. **83**, 3780 (1999).